# A fixed-switching-frequency Sliding Mode Current Controller for Mutually Coupled Switched Reluctance Machines using Asymmetric Bridge Converter

Kun Hu, Jin Ye, Javad Mohammadpour Velni, Lulu Guo and Bowen Yang School of Electrical and Computer Engineering University of Georgia, Athens, Georgia 30602

Email: kun.hu@uga.edu, jin.ye@uga.edu, javadm@uga.edu, lulu.guo@uga.edu, bowen.yang@uga.edu

Abstract—In this paper, an integral sliding mode current controller (SMC) is proposed for mutually coupled switched reluctance motors (MCSRM) using asymmetric bridge converters aiming to achieve constant switching frequency and lower sampling rate. A generalized state-space model is built and then the design of a sliding mode controller along with the stability analysis of the closed-loop system are presented. The effectiveness of SMC is verified using simulation studies with a three-phase, sinusoidal excitation 12/8 MCSRM over a wide speed range. Compared to the hysteresis current control, the proposed SMC-based design approach demonstrates a comparable response in terms of currents ripples, the root-mean-square error of current and torque while achieving a constant switching frequency and lower sampling rate.

#### I. INTRODUCTION

As potentially rare-earth-free substitutes of conventional electric machines, mutually coupled switched reluctance motors (MCSRMs) show great promise in electrified transportation, industrial applications, and home appliances. They retain important benefits of conventional switched reluctance machines (CSRMs), including their rigidity, non-reliance on rare-earth permanent magnet materials, and extended-speed constant-power range [1]–[3]. Since the winding current can flow bidirectionally, the motor can be driven by a six-switch standard converter, which has a wide range of applications in industry. In addition to the above benefits, several distinctive advantages of MCSRMs should be considered, for instance, lower copper and iron losses, higher fault-tolerance and less sensitivity to magnetic saturation [4]–[7].

Normally, an MCSRM can be driven by both conventional asymmetric bridge converter (with unipolar current excitation) and three-phase standard inverter (with either bipolar square-waveform or sinusoidal-waveform current excitations) [8]. Among the current control methods for different converter topologies, current hysteresis control has been widely used in conventional switched reluctance motor (CSRM) and MCSRM drives due to its simplicity, fast dynamic response, and independence of motor models. However, this method suffers from variable switching frequency and much higher sampling rate in the digital implementation. To overcome these drawbacks,

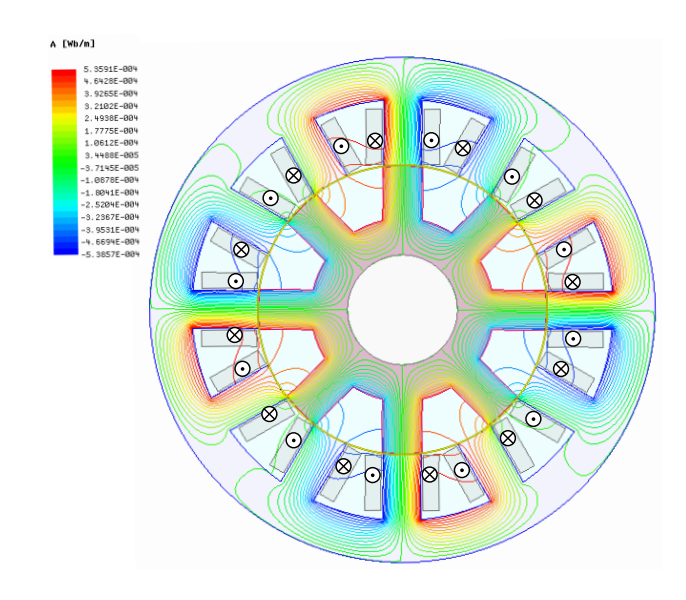


Fig. 1. Topology of a short-pitched MCSRM.

some constant-switching-frequency current controllers were developed in [2] for conventional SRMs, but to the best of our knowledge, no work has been done on achieving constant switching frequency current control for MCSRMs because of the extreme nonlinearity and mutual coupling. The closest works are the sliding mode current control for conventional SRMs [9]–[11], in which the mutual coupling impact are relatively small and often neglected. Therefore, previous works cannot be directly applied to MCSRMs because of the considerable mutual coupling.

Generally speaking, MCSRMs can be categorized as short-pitched, full-pitched and fractionally-pitched MCSRMs, and each has different mutual and self-inductance profiles due to various winding distributions. In this paper, through the design and tuning of the sliding mode controller, a constant switching frequency current controller is proposed for a short-pitched MCSRM to address the above issues. The winding distribution is shown in Fig. 1. The paper is organized as

follows. In section II, the relationship between switching frequency and current ripple is derived through general mathematical modeling of a MCSRM driven by asymmetric bridge converter. Section III presents the problem formulation of the sliding mode control, wherein the variable switching frequency issue caused by traditional hysteresis current controllers is addressed. Moreover, to demonstrate the robustness of sliding mode controller, stability analysis of the closed loop is presented. Then, comparison results are shown in section IV to validate the effectiveness of the proposed sliding mode current controller, and conclusions are given in section V.

#### II. MODELING OF MCSRM

The phase voltage equations for the investigated three-phase MCSRMs are given by [2]

$$\begin{bmatrix} v_{k-1} \\ v_k \\ v_{k+1} \end{bmatrix} = T \begin{bmatrix} i_{k-1} \\ i_k \\ i_{k+1} \end{bmatrix} + \Lambda \begin{bmatrix} \frac{d}{dt}i_{k-1} \\ \frac{d}{dt}i_k \\ \frac{d}{dt}i_{k+1} \end{bmatrix}$$
(1)

where T and  $\Lambda$  are defined as

where 
$$T$$
 and  $\Lambda$  are defined as 
$$T = \begin{bmatrix} R + \frac{\partial L_{k-1}}{\partial \theta} \omega_m & \frac{\partial M_{k(k-1)}}{\partial \theta} \omega_m & \frac{\partial M_{(k-1)(k+1)}}{\partial \theta} \omega_m \\ \frac{\partial M_{k(k-1)}}{\partial \theta} \omega_m & R + \frac{\partial L_k}{\partial \theta} \omega_m & \frac{\partial M_{k(k+1)}}{\partial \theta} \omega_m \\ \frac{\partial M_{(k-1)(k+1)}}{\partial \theta} \omega_m & \frac{\partial M_{k(k+1)}}{\partial \theta} \omega_m & R + \frac{\partial L_{k+1}}{\partial \theta} \omega_m \end{bmatrix}$$

$$\Lambda = \begin{bmatrix} L_{k-1} & M_{k(k-1)} & M_{(k-1)(k+1)} \\ M_{k(k-1)} & L_k & M_{k(k+1)} \\ M_{(k-1)(k+1)} & M_{k(k+1)} & L_{k+1} \end{bmatrix}.$$

Where R is ohmic resistance;  $v_j, i_j, L_j$  are phase voltage, current, and self-inductance of jth phase (j=k-1,k,k+1), respectively;  $\theta$  is rotor angle; and  $\omega_m$  is angular speed. Since the mutual inductances between two conducting phases are the same, e.g.,  $M_{(k-1)(k+1)} = M_{(k+1)(k-1)}$ , we use  $M_{(k-1)k}, M_{(k-1)(k+1)}$  and  $M_{k(k+1)}$  to denote the mutual inductances among the adjacent conducting phases.

Fig. 2 shows the self-inductance and mutual inductance profiles of the short-pitched MCSRM with single phase current excitation, which is obtained from 2D finite element analysis (FEA). It can be observed that the MCSRM contains non negligible negative mutual inductance compared to the conventional SRM. Fig. 3 shows the different flux path pattern of MCSRM and conventional ones with one phase excited. We can observe that for the MCSRM, the flux in the active phase splits into two directions and flows back through the adjacent stator poles, while flux in the CSRM goes through a longer path before eventually gathering in the active phase [12]. The unique flux pattern of MCSRM can alleviate the saturation in the core back which is indicated from Fig. 3 with lower flux density in MCSRM. However, such short flux path of the investigated MCSRM results in significant mutual coupling of the adjacent phases, especially for the case that the mutual inductance is of negative polarity, which brings significant consequence of higher switching rate for the asymmetric bridge converter.

For the CSRM, at the initial stage, the switching frequency of the kth phase can be expressed as (2). The maximum

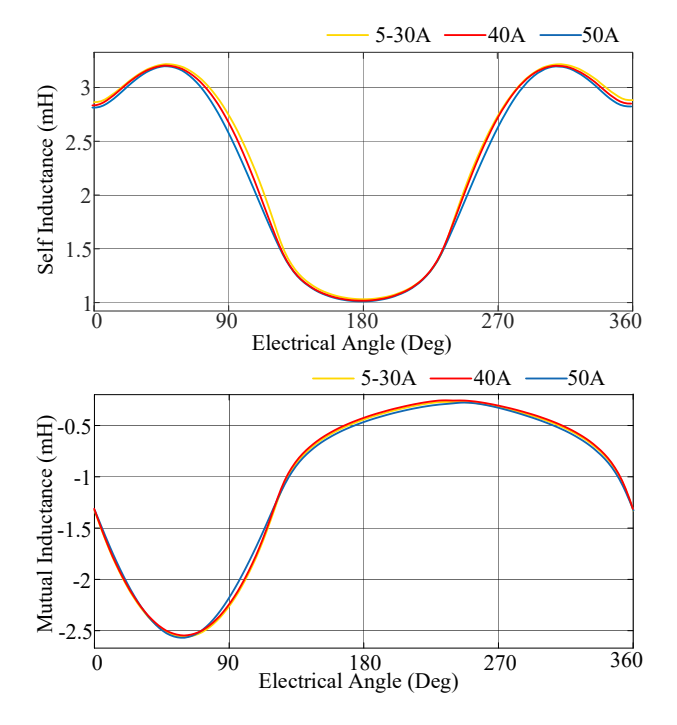


Fig. 2. Inductance profiles of the investigated MCSRM.

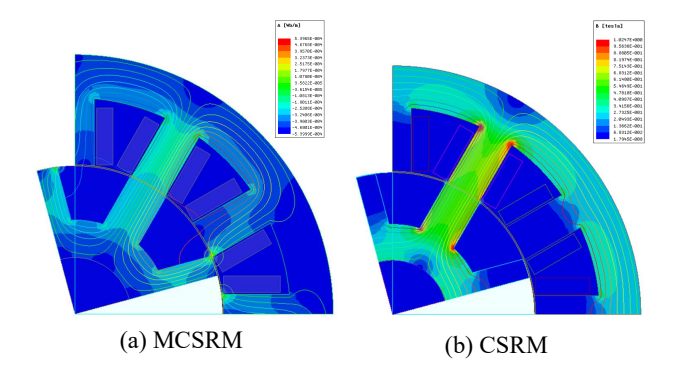


Fig. 3. Different flux path patterns of MCSRM and CSRM.

 $f_{k_{CSRM}}$  is achieved at minimum self-inductance when the DC voltage and current ripple band are fixed.

$$v_k \approx L_k \frac{di_k}{dt_k}, \ f_{k_{CSRM}} = \frac{1}{\Delta t_k} = \frac{v_k}{2L_k \Delta i_k}.$$
 (2)

Different from the CSRM, in an MCSRM, the switching frequency derivation of the kth phase involves mutual inductance induced by conducting (k-1)th and (k+1)th phases shown in (3). The asymmetric bridge converter makes it possible that the current variation of the three phases are of the same signs. Assuming that the switching frequencies for the three phases are close and that the required current bands for the three phases are the same, the highest switching frequency  $f_{k_{MCSRM}}$  is obtained when the current variations are of the same sign shown in (4). It is noticeable that the sum of the inductances  $L_k, M_{k(k+1)}$  and  $M_{k(k-1)}$  is much lower than  $L_k$  alone in

(2). Therefore,  $f_{k_{MCSRM}}$  is much larger than  $f_{k_{CSRM}}$ 

Therefore, 
$$f_{k_{MCSRM}}$$
 is much larger than  $f_{k_{CSRM}}$ .
$$v_k \approx L_k \frac{di_k}{dt_k} + M_{k(k-1)} \frac{di_{k-1}}{dt_{k-1}} + M_{k(k+1)} \frac{di_{k+1}}{dt_{k+1}}, \quad (3)$$

$$f_{k_{MCSRM}} \approx \frac{v_k}{2(L_k + M_{k(k+1)} + M_{k(k+1)})\Delta i_k}. \quad (4)$$

$$f_{k_{MCSRM}} \approx \frac{v_k}{2(L_k + M_{k(k+1)} + M_{k(k-1)})\Delta i_k}.$$
 (4)

Referring to the FEA result of the studied MCSRM, the sum of  $L_k$ ,  $M_{k(k+1)}$  and  $M_{k(k-1)}$  at every time instant varies from  $190\mu H$  to  $720\mu H$ , which leads to a minimum 50k-switching frequency when the current band is 1A and DC voltage is 72V. Therefore, the existence of the negative mutual inductance in the investigated MCSRM posts a high switching frequency demand for the converter. Consequently, the required control frequency is high as well.

It can be seen from Fig. 2 that the investigated MCSRM is not magnetic saturated when phase A is excited with 1.5 times of the rated current. Therefore, the total electromagnetic torque of the n-phase MCSRM working in the linear magnetic region is given by

$$T = \frac{1}{2} \frac{\partial L_{k-1}}{\partial \theta} i_{k-1}^2 + \frac{1}{2} \frac{\partial L_k}{\partial \theta} i_k^2$$

$$+ \frac{1}{2} \frac{\partial L_{k+1}}{\partial \theta} i_{k+1}^2 + \frac{\partial M_{k(k-1)}}{\partial \theta} i_{k-1} i_k$$

$$+ \frac{\partial M_{k(k+1)}}{\partial \theta} i_k i_{k+1} + \frac{\partial M_{(k-1)(k+1)}}{\partial \theta} i_{k-1} i_{k+1}.$$
 (5)

In this section, we describe the design process of the proposed SMC-based controller and then provide stability analysis for the closed-loop system of the SMC control scheme and the MCSRM.

#### A. Design of sliding mode controller

To address the variable switching frequency issue for MC-SRM, sliding mode current controller is proposed in this work. Based on the motor voltage equation (1), the state-space dynamics of the current control system can be derived as

$$\dot{e} = -Ae + Ai_{ref} - Bv, \tag{6}$$

where the current errors associated with the three phases form the state vector e, the voltage associated with the three phases form the control input vector v, and A, B and e are defined by

$$A = B\Lambda, \ B = T^{-1},$$

$$e = \begin{bmatrix} e_{k-1} \\ e_k \\ e_{k+1} \end{bmatrix} = \begin{bmatrix} i_{ref_{k-1}} - i_{k-1} \\ i_{ref_k} - i_k \\ i_{ref_{k+1}} - i_{k+1} \end{bmatrix}.$$

An integral switching surface for the conducting phases is chosen as

$$s(t) = e(t) + \alpha \int e(t)dt. \tag{7}$$

To force s to slide along the restricted sliding surface s = 0, the dynamics of the sliding mode s are designed as follows:

$$\dot{s} = -qs + \varepsilon \operatorname{sgn}(s),\tag{8}$$

$$\varepsilon = \begin{bmatrix} \varepsilon_{k-1} & 0 & 0 \\ 0 & \varepsilon_k & 0 \\ 0 & 0 & \varepsilon_{k+1} \end{bmatrix}, \ s = \begin{bmatrix} s_{k-1} & s_k & s_{k+1} \end{bmatrix}^T,$$

$$\alpha = \begin{bmatrix} \alpha_{k-1} & 0 & 0 \\ 0 & \alpha_k & 0 \\ 0 & 0 & \alpha_{k+1} \end{bmatrix}, \ q = \begin{bmatrix} q_{k-1} & 0 & 0 \\ 0 & q_k & 0 \\ 0 & 0 & q_{k+1} \end{bmatrix},$$

$$\operatorname{sgn}(s) = \begin{bmatrix} \operatorname{sgn}(s_{k-1}) & \operatorname{sgn}(s_k) & \operatorname{sgn}(s_{k+1}) \end{bmatrix}^T,$$

wherein, the gains  $a, q, \varepsilon$  for each phase are positive to ensure the convergence of sliding mode and current error. Then, by combing (6)-(8), the control input v can be derived as

$$v = B^{-1}(qs + \varepsilon \operatorname{sgn}(s) - Ae + Ai_{ref} - Bv), \tag{9}$$

and the duty cycle for each phase can be derived by

$$d = \begin{bmatrix} d_{k-1} \\ d_k \\ d_{k+1} \end{bmatrix} = \begin{bmatrix} s_{k-1} \\ s_k \\ s_{k+1} \end{bmatrix} v_{dc}, \tag{10}$$

where  $v_{dc}$  denotes the DC link voltage

### B. Stability analysis of the closed-loop system

When the motor parameter uncertainties are neglected, the closed-loop system dynamics can be derived by combining the current error dynamics and sliding mode control dynamics as

$$\dot{X} = A_1 X + B_1 U,\tag{11}$$

where  $B_1$  is the identity matrix, and X, U and  $A_1$  are defined

$$X = \begin{bmatrix} s_{k-1} \\ s_k \\ s_{k+1} \\ e_{k-1} \\ e_k \\ e_{k+1} \end{bmatrix}, \quad U = \begin{bmatrix} -\varepsilon_{k-1} \operatorname{sgn}(s_{k-1}) \\ -\varepsilon_{k} \operatorname{sgn}(s_k) \\ -\varepsilon_{k+1} \operatorname{sgn}(s_{k+1}) \\ e_{k-1} \\ e_k \\ e_{k+1} \end{bmatrix},$$

$$A_1 = \begin{bmatrix} -q_{k-1} & 0 & 0 & 0 & 0 & 0 \\ 0 & -q_k & 0 & 0 & 0 & 0 \\ 0 & 0 & -q_{k+1} & 0 & 0 & 0 \\ -q_{k-1} & 0 & 0 & -\alpha_{k-1} & 0 & 0 \\ 0 & 0 & -q_{k+1} & 0 & 0 & -\alpha_{k+1} \end{bmatrix}.$$

Then, the stability of the system in (11) can be proved using Lyapunov stability theory as follows. The Lyapunov function is chosen as

$$V(X) = X^T P X, (12)$$

where P is the positive definite solution t the following:

$$A_1^T P + P A_1 = -I. (13)$$

Then, the first-order derivative of V(X) is

$$\dot{V}(X) = \dot{X}^T P X + X^T P \dot{X} 
= \dot{X} (A_1^T P + P A_1) X + 2 U^T B_1^T P X 
= - || x ||^2 + 2 U^T B_1^T P X.$$
(14)

If U in the above equations is bounded and X is large enough,  $\dot{V}(X)$  is then negative. In other words, bounded X can make the system bounded-input and bounded-output (BIBO) stable. Therefore, to ensure the BIBO stability, a positive definite P should be obtained by solving (13), which gives

$$P = \begin{bmatrix} p_{11} & 0 & 0 & p_{14} & 0 & 0 \\ 0 & p_{22} & 0 & 0 & p_{25} & 0 \\ 0 & 0 & p_{33} & 0 & 0 & p_{36} \\ p_{41} & 0 & 0 & p_{44} & 0 & 0 \\ 0 & p_{52} & 0 & 0 & p_{55} & 0 \\ 0 & 0 & p_{63} & 0 & 0 & p_{66} \end{bmatrix}, \quad (15)$$

where

$$\begin{split} p_{11} &= \frac{(\alpha_{k-1} + q_{k-1})\alpha_{k-1} + q_{k-1}^2}{2(\alpha_{k-1} + q_{k-1})\alpha_{k-1}q_{k-1}}, p_{44} = \frac{1}{2\alpha_{k-1}}, \\ p_{22} &= \frac{(\alpha_k + q_k)\alpha_k + q_k^2}{2(\alpha_k + q_k)\alpha_kq_k}, p_{55} = \frac{1}{2\alpha_k}, \\ p_{33} &= \frac{(\alpha_{k+1} + q_{k+1})\alpha_{k+1} + q_{k+1}^2}{2(\alpha_{k+1} + q_{k+1})\alpha_{k+1}q_{k+1}}, p_{66} = \frac{1}{2\alpha_{k+1}}, \\ p_{14} &= p_{41} = \frac{-q_{k-1}}{2(\alpha_{k-1} + q_{k-1})\alpha_{k-1}q_{k-1}}, \\ p_{25} &= p_{52} = \frac{-q_k}{2(\alpha_k + q_k)\alpha_kq_k}, \\ p_{36} &= p_{63} = \frac{-q_{k+1}}{2(\alpha_{k+1} + q_{k+1})\alpha_{k+1}q_{k+1}}. \end{split}$$

To ensure that P is positive definite, selection of the parameters  $\alpha$  and q for the sliding mode controller is guided with the following conditions:

$$\begin{split} &\frac{(\alpha_{k-1}+q_{k-1})\alpha_{k-1}+q_{k-1}^2}{2(\alpha_{k-1}+q_{k-1})\alpha_{k-1}q_{k-1}}>0,\ \frac{(\alpha_k+q_k)\alpha_k+q_k^2}{2(\alpha_k+q_k)\alpha_kq_k}>0,\\ &\frac{(\alpha_{k+1}+q_{k+1})\alpha_{k+1}+q_{k+1}^2}{2(\alpha_{k+1}+q_{k+1})\alpha_{k-1}q_{k-1}}>0,\\ &\frac{(\alpha_{k-1}+q_{k-1})^2+q_{k-1}^2}{4(\alpha_{k-1}+q_{k-1})^2\alpha_{k-1}q_{k-1}}>0,\ \frac{(\alpha_{k-1}+q_k)^2+q_k^2}{4(\alpha_k+q_k)^2\alpha_kq_k}>0,\\ &\frac{(\alpha_{k+1}+q_{k+1})^2+q_{k+1}^2}{4(\alpha_{k+1}+q_{k+1})^2\alpha_{k+1}q_{k+1}}>0, \end{split}$$

when neglecting the motor model parameter uncertainties.

## IV. SIMULATION RESULTS AND PERFORMANCE EVALUATION

In this section, the performance of the proposed sliding mode current controller is compared to hysteresis current controller in terms of RMSE current and torque, RMS current and torque ripple which are defined as

$$I_{RMSE} = \sqrt{\frac{1}{\theta_p} \int_0^{\theta_p} (i_{ref} - i_k)^2 d\theta}$$
 (16)

$$I_{RMS} = \sqrt{\frac{1}{\theta_p} \int_0^{\theta_p} i_k^2 d\theta}$$
 (17)

$$T_{RMSE} = \sqrt{\frac{1}{\theta_p} \int_0^{\theta_p} (T_{e-ref} - T_e)^2 d\theta}$$
 (18)

$$T_{rip} = \frac{T_{max} - T_{min}}{T_{ave}} \tag{19}$$

where  $\theta_p=2\pi/N_p$  is determined based on the number of rotor poles. The current references are the three phase sinusoidal waveforms given by

$$\begin{cases}
I_{ref_A} = I_m \sin[N_p(\omega t - \delta)] \\
I_{ref_B} = I_m \sin[N_p(\omega t - 30^\circ - \delta)] \\
I_{ref_C} = I_m \sin[N_p(\omega t + 30^\circ - \delta)]
\end{cases}$$
(20)

and the amplitude of the sinusoidal current reference is set to be 15 A and the leading angle is  $2^{\circ}$ .

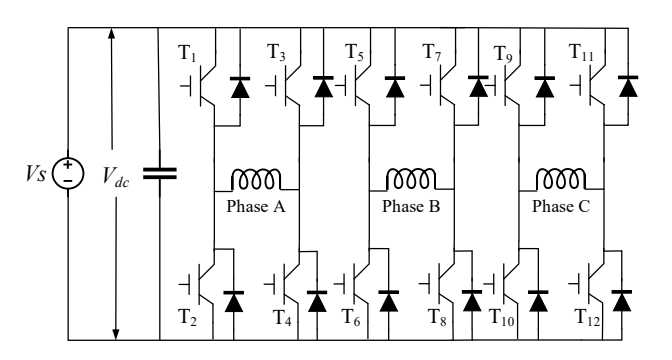


Fig. 4. Asymmetric bridge converter.

As described in Section II, the switching frequency is relatively high for the investigated MCSRM driven by the asymmetric bridge converter shown in Fig. 4. For hysteresis current control, the current hysteresis band is set as 2A and the sampling rate  $f_c$  of the current feedback is set as 100 kHz to limit the switching frequency  $f_s$  around 50 kHz. For fair comparison, the switching frequency of the PWM using SMC is firstly set as 50 kHz and the sampling rate is set as 100 kHz, then the sampling rate is set as 50 kHz. The parameters of the sliding mode current controller are chosen as

$$\begin{cases}
\alpha_{k-1} = \alpha_k = \alpha_{k+1} = 50000 \\
q_{k-1} = q_k = q_{k+1} = 100 \\
\varepsilon_{k-1} = \varepsilon_k = \varepsilon_{k+1} = 10.
\end{cases}$$
(21)

Figures 5 and 6 illustrate the current and torque trajectories at 2200 rpm under the same switching frequency (50 kHz) and sampling rate (100 kHz). Compared to the conventional hysteresis current controller, SMC shows comparable performance while resulting in a smoother current feedback. It can be seen from Table I that MCSRM with hysteresis current

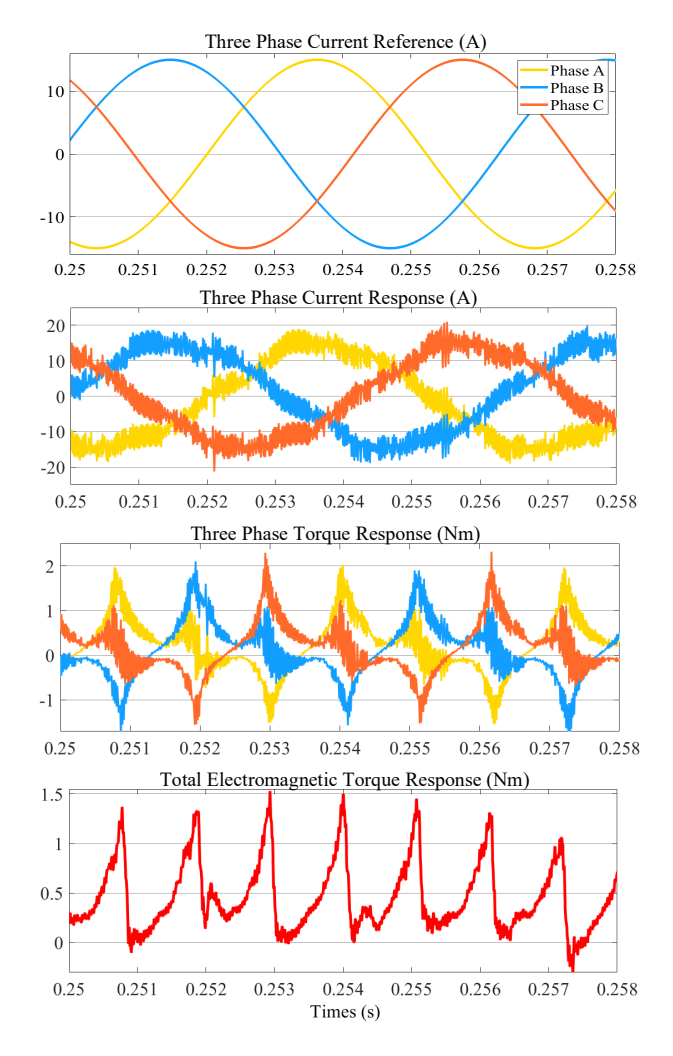


Fig. 5. Simulation results with hysteresis current controller.

TABLE I
COMPARISON OF THE PERFORMANCE OF THE TWO CURRENT
CONTROLLERS.

Hysteresis current controller $(f_s \approx 50k, f_c = 100k)$			
$I_{RMS}$	$I_{RMSE}$	$T_{RMSE}$	$T_{rip}$
10.50	2.04	0.23	526%
10.62	1.95	0.28	411%
10.23	2.03	0.25	557%
10.01	2.44	0.34	392%
Sliding mode current controller $(f_s = 50k, f_c = 50k)$			
$I_{RMS}$	$I_{RMSE}$	$T_{RMSE}$	$T_{rip}$
10.79	3.30	0.04	330%
10.65	2.41	0.06	317%
10.58	2.88	0.07	307%
10.96	4.68	0.15	328%
Sliding mode current controller $(f_s = 50k, f_c = 100k)$			
$I_{RMS}$	$I_{RMSE}$	$T_{RMSE}$	$T_{rip}$
10.37	1.66	0.02	322%
10.39	1.48	0.04	309%
10.33	1.73	0.06	307%
10.68	3.50	0.17	303%
	$\begin{array}{c} I_{RMS} \\ 10.50 \\ 10.62 \\ 10.23 \\ 10.01 \\ \text{Sliding} \\ I_{RMS} \\ 10.79 \\ 10.65 \\ 10.58 \\ 10.96 \\ \text{Sliding r} \\ I_{RMS} \\ 10.37 \\ 10.39 \\ 10.33 \\ \end{array}$	$\begin{array}{c cccc} I_{RMS} & I_{RMSE} \\ \hline 10.50 & 2.04 \\ 10.62 & 1.95 \\ 10.23 & 2.03 \\ 10.01 & 2.44 \\ \hline Sliding mode curren \\ \hline I_{RMS} & I_{RMSE} \\ \hline 10.79 & 3.30 \\ 10.65 & 2.41 \\ 10.58 & 2.88 \\ \hline 10.96 & 4.68 \\ \hline Sliding mode current \\ \hline I_{RMS} & I_{RMSE} \\ \hline 10.37 & 1.66 \\ 10.39 & 1.48 \\ \hline 10.33 & 1.73 \\ \hline \end{array}$	$\begin{array}{c ccccccccccccccccccccccccccccccccccc$

controller bears more significant torque ripples of around 450% and higher torque RMSE, while MCSRM controlled by SMC under two sampling rates carries lower torque ripples of

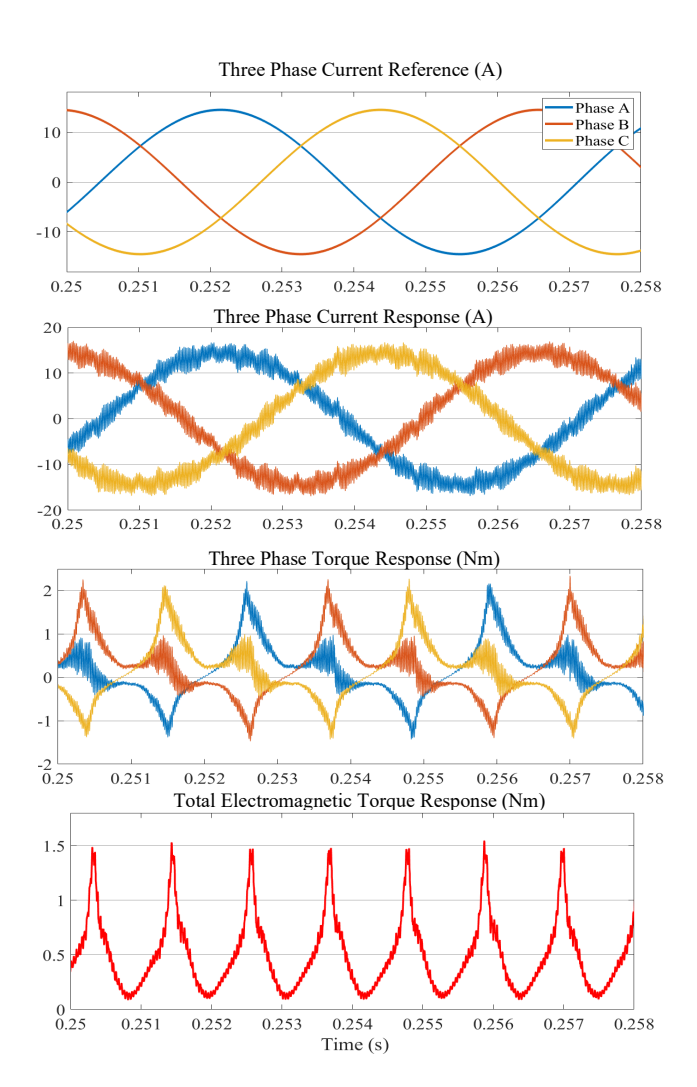


Fig. 6. Simulation results with sliding mode current controller.

around 300% and lower torque RMSE value which is less than 0.1Nm over a wide speed range. The data shown in the table also demonstrates that with the same switching frequency and sampling frequency, both methods yield comparable current RMSE values of 2A which agrees with the theoretical analysis. In addition, decreasing the sampling rate will worsen performance for both controllers, causing higher current ripples and torque fluctuations. The simulation results of hysteresis current control with 50kHz sampling rates are not presented in this paper as the current and torque fluctuations are too severe. To summarize, SMC scheme results in a more robust performance when the sampling rate is lower. Furthermore, SMC offers advantages over hysteresis current control in terms of fixed switching frequency and lower sampling rates.

#### V. CONCLUSION

In this paper, the mathematical modeling and analysis revealed the fact that the asymmetric bridge converters used for the investigated short-pitched MCSRM demands a relatively high switching rate in order to maintain good current control performance. The integral sliding mode control method was

proposed in this work for the current control system aiming to achieve a fixed switching rate and lower sampling rate. The stability analysis of the closed loop system with SMC and the parameter selection of the SMC was provided. Simulation results comparing to the hysteresis current controller validated the effectiveness and advantages of sliding mode control in terms of constant switching frequency and lower sampling rates. For the future work, further investigation is needed to reduce the switching frequency for the investigated MCSRM drive system.

#### ACKNOWLEDGMENT

This work is partially supported by NSF-ECCS-1725636 and NSF-ECCS-1851875.

#### REFERENCES

- F. Peng, J. Ye, and A. Emadi, "A digital pwm current controller for switched reluctance motor drives," *IEEE Transactions on Power Electronics*, vol. 31, no. 10, pp. 7087–7098, 2016.
- [2] J. Ye, P. Malysz, and A. Emadi, "A fixed-switching-frequency integral sliding mode current controller for switched reluctance motor drives," *IEEE Journal of Emerging and Selected Topics in Power Electronics*, vol. 3, no. 2, pp. 381–394, 2015.
- [3] F. Yi and W. Cai, "Modeling, control, and seamless transition of the bidirectional battery-driven switched reluctance motor/generator drive based on integrated multiport power converter for electric vehicle applications," *IEEE Transactions on Power Electronics*, vol. 31, no. 10, pp. 7099–7111, 2016.
- [4] G. Li, J. Ojeda, E. Hoang, M. Lécrivain, and M. Gabsi, "Comparative studies between classical and mutually coupled switched reluctance motors using thermal-electromagnetic analysis for driving cycles," *IEEE Transactions on magnetics*, vol. 47, no. 4, pp. 839–847, 2011.
- [5] W. Ding, Y. Hu, and L. Wu, "Investigation and experimental test of fault-tolerant operation of a mutually coupled dual three-phase srm drive under faulty conditions," *IEEE Transactions on Power Electronics*, vol. 30, no. 12, pp. 6857–6872, 2015.
- [6] G. Li, X. Ojeda, S. Hlioui, E. Hoang, M. Gabsi, and C. Balpe, "Comparative study of switched reluctance motors performances for two current distributions and excitation modes," in 2009 35th Annual Conference of IEEE Industrial Electronics. IEEE, 2009, pp. 4047– 4052.
- [7] R. Pupadubsin, N. Chayopitak, S. Karukanan, P. Champa, P. Somsiri, and K. Tungpimolrut, "Comparison of winding arrangements of three phase switched reluctance motor under unipolar operation," in 2012 15th International Conference on Electrical Machines and Systems (ICEMS). IEEE, 2012, pp. 1–4.
- [8] V. Rallabandi, S. Mallampalli, R. Rahul, and D. Torrey, "Performance comparison of switched reluctance motor with sinusoidal and conventional excitation," in 2015 IEEE Energy Conversion Congress and Exposition (ECCE). IEEE, 2015, pp. 5580–5585.
- [9] M. Falahi and F. R. Salmasi, "A sliding mode controller for switchedreluctance motor with iterative learning compensation," in 2007 International Conference on Electrical Machines and Systems (ICEMS). IEEE, 2007, pp. 631–635.
- [10] S. Sahoo, S. Panda, and J. Xu, "Direct torque controller for switched reluctance motor drive using sliding mode control," in 2005 International Conference on Power Electronics and Drives Systems, vol. 2. IEEE, 2005, pp. 1129–1134.
- [11] M. N. Isfahani, S. Saghaian-Nejad, A. Rashidi, and H. A. Zarchi, "Passivity-based adaptive sliding mode speed control of switched reluctance motor drive considering torque ripple reduction," in 2011 IEEE International Electric Machines & Drives Conference (IEMDC). IEEE, 2011, pp. 1480–1485.
- [12] X. Deng, B. Mecrow, R. Martin, and S. Gadoue, "Effects of winding connection on performance of a six-phase switched reluctance machine," *IEEE Transactions on Energy Conversion*, vol. 33, no. 1, pp. 166–178, 2018